Construction of a Cavity Ring-Down Spectroscopy System for Rare Event Searches

E. E. Deck[1], A. W. Johnson [2] , B. J. Mount[3]
1 - Department of Physics, University of California, Berkeley, 366 LeConte Hall, Berkeley, CA 94720
2-Science Department, Belle Fourche Middle School, 1302 Ziebach Street, Belle Fourche, SD, 57717
3- School of Natural Sciences, Black Hills State University, Spearfish, SD 57783

Introduction:

Rare event searches, such as the LUX-ZEPLIN dark matter experiment (see Fig. 1), involve using a Time Projection Chamber (TPC) filled with a liquid noble gas as a detection medium in order to sense rarely occurring particle interactions. TPCs produce particle detection signals by observing both photons and electrons emitted as a consequence of particles interacting with the liquid noble gas [1,2]. Trace-level impurities in the detection medium reduce the sensitivity of the detector by interfering with the ability of the emitted photons and electrons to traverse the length of the TPC and be measured by photomultiplier tube arrays at the TPC's ends [3]. Extremely precise purity measurements are necessary to ensure the extreme sensitivity of the rare event search. A Cavity Ring-Down Spectroscopy (CRDS) system is being developed to detect ultra-trace impurities at the parts-per-trillion level [4,5,6]. As the detection medium is utilized, it requires ongoing purification procedures. An in-line CRDS system would allow continuous, non-destructive measurement of TPC purity.

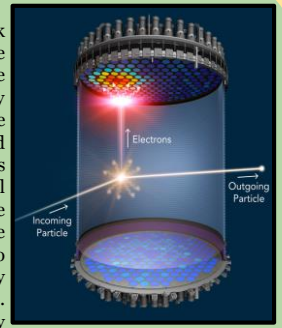

Fig 1: A diagram of the LUX-Zeplin Liquid Xenon Time Projection Chamber (Image courtesy LZ Collaboration)

CRDS Overview:

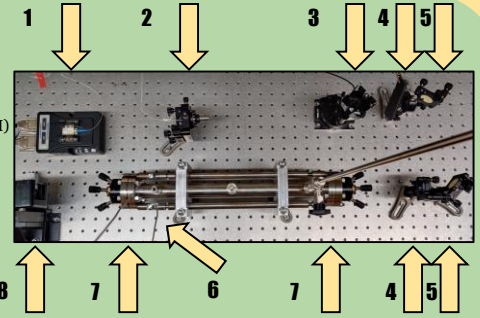

1: 1650 nm Laser
2: Fiber-to-free-space Collimator
2: Acousto-Optic Modulator(AOM)
3: Focusing Lens
3: Alignment Mirror
4: "Super" (High-R) Mirror
5: Optical Detector
6: Piezoelectric Transducers

Fig 2. The layout of the CRDS system

Cavity Ring-Down Spectroscopy (CRDS) is a high-precision optical spectroscopy technique[7,8]. In the BHSU CRDS system, (see fig 2.), the beam from a 1650nm laser is passed through an AOM, which allows rapid (<10ns [9]) control of the incidence of light into the cavity. The beam then passes through two focusing lenses and two alignment mirrors, which control the beam geometry. Two piezo-electric transducers allow varying voltage to "tune" the cavity length so that a standing wave forms. The buildup of light is measured by the optical detector and once a threshold of light intensity is surpassed, light input is abruptly stopped. The so-called "ring-down" time of light decay within the cavity is measured (see figs. 3.1-3), which is evaluated as a metric of the optical extinction coefficient of the sample and cavity [8]. Comparison of this data to reference allows for quantification of the analyte present. This process repeats itself automatically, allowing for many trials to occur, independent of manual control.

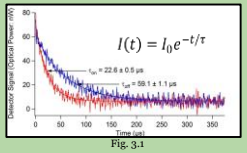

Fig. 3.1

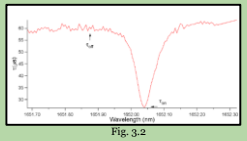

Fig. 3.2

$$N = \frac{1}{c\sigma^2}\left(\frac{1}{\tau(\lambda_{on})} - \frac{1}{\tau(\lambda_{off})}\right)$$

Fig. 3.3

Fig 3.1 An example ring-down analysis. Ring-down on resonance (red) is compared to off resonance (blue).
Fig. 3.2 Ring-down compared to frequency.
Fig 3.3 Formula used to derive the concentration of the analyte.

Optical Properties of CRDS:

A CRDS system is defined by several parameters fundamental to the cavity design (see table). During the design and construction process, each must be chosen to maximize the cavity's sensitivity to a particular impurity (in this case, methane) and also for physical considerations (length of the optical bench, etc.). Mirrors with sufficiently high reflectivity placed an appropriate length apart constitute the cavity.

Table 1: The fundamental parameters of the cavity (L, R, and λ) and the quantities derived from them (f, δν, and L_eff)

Cavity Length	L	0.4m
Reflectivity	R	0.99997079
Wavelength	λ	1652.10nm
Finesse	$f \equiv \frac{\pi\sqrt{R}}{(1-R)}$	107,550
Free Spectral Range	$\delta\nu_{FSR} \equiv \frac{c}{2L}$	375MHz
Effective Length	$L_{eff} \equiv \frac{L}{1-R}$	13.693km

$$I = I_0 e^{-N\cdot\sigma(\nu)\cdot d} \quad | \quad I(t) = I_0 e^{\frac{-c(1-R)}{L}\cdot t}$$

$$I(t) = I_0 e^{\frac{-tc}{L}(1-R+N\cdot\sigma(\nu)\cdot d)}$$

$$\tau \equiv \frac{L}{c(1-R+N\cdot\sigma(\nu)\cdot d)}$$

Fig. 4. The Derivation of the "ring-down time" (τ) from the Beer-Lambert law and Cavity ring-down time [10]

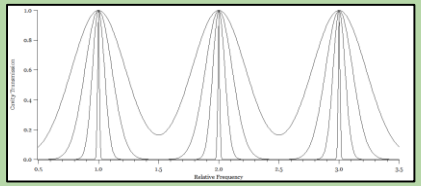

Fig. 5. A graph showing decreasing mode width as reflectivity (R) and finesse (*f*) increase. The distance between peaks is FSR, and the peak width is finesse.

Various measures of cavity performance can then be calculated. The first is the cavity's finesse, a measure of the degree to which the optical cavity can sustain constructive interference over the effective path length of the cavity [4]. Another is the cavity's free spectral range, which is the frequency spacing between adjacent modes (see fig 6). The last is the cavity's effective path length, which is a measure of the distance a typical photon would travel before scattering or absorption. The longer the effective path length, the greater the sensitivity of the ring-down time measurement.

Beam Profiling:

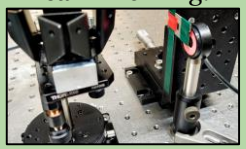

Fig. 6. A knife-edge beam profiling configuration, featuring an AOM, Micrometer mounted razor, and Power Meter

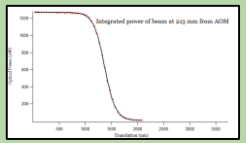

Fig. 7. Sample Data for Beam profiling at 213mm displacement from AOM

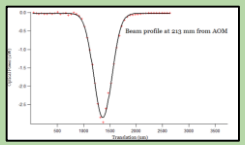

Fig. 8. Sample Data for Beam Profile at 213mm, differentiated to show Gaussian profile

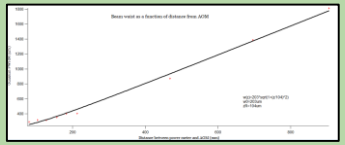

Fig. 9. Beam waist as a function of distance from AOM

As the beam exits the AOM, its radius varies as a function of distance. In order to understand the beam's geometry for mode-matching purposes, measurements were taken using the knife edge beam profiling method (see fig 6.)[11]. In this process, the beam's power is recorded as a micrometer-mounted razor is lowered into the beam. This yields the beam's integrated power as differing amounts of it are cut-off (see fig. 6). By repeating this process at multiple distances from the AOM, and differentiating the resultant data, gaussian fits are found for the beam's power (see fig. 7)[12].

By taking the derived Full-Width Half-Maximum (FWHM) measurement for the beam's gaussian distribution at several distances from the AOM, a curve that defines the beam's profile can be developed (see figs. 9 and 10). Two of the fit parameters -- the beam's natural waist and Rayleigh range -- are used to define the beam's evolution in free space. These go on to define the mode matching; enabling us to place necessary focusing lenses correctly.

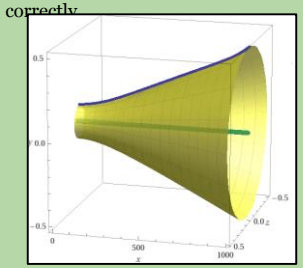

Fig. 10. A visualization of the beam shape over distance (mm) from AOM

Mode Matching:

Within the cavity, there are multiple possible modes of optical stability (see fig. 11). In order to have clear ring-downs, it is necessary to maximize the amount of light in one mode and minimize the others, so as toavoid interference [13]. In order to do this, the beam geometry (measured in Beam Profiling) must be converted to that "desired" by our chosen mode by the placement of lenses. The determination of the appropriate lens focal length and distance from various optics can be made using ray matrix optics -- in which the beam's propagation and interaction with optics is modeled as a series of transfer matrices. Leaving the necessary constraints as variables, the system can be computationally optimized using MatLab.

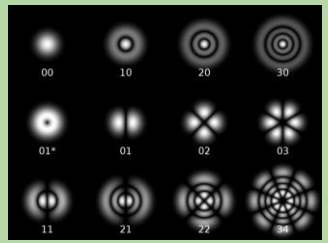

Fig. 11. 2D representation of several low-order modes of optical resonance within our cylindrically-symmetrical cavity. Image courtesy Wikimedia Commons

$$\begin{bmatrix} A & B \\ C & D \end{bmatrix} = \begin{bmatrix} 1 & 0 \\ 0 & \frac{n_2}{n_1} \end{bmatrix}\begin{bmatrix} 1 & d \\ 0 & 1 \end{bmatrix}\begin{bmatrix} 1 & 0 \\ 0 & \frac{n_1}{n_2} \end{bmatrix}\begin{bmatrix} 1 & x_3 \\ 0 & 1 \end{bmatrix}\begin{bmatrix} 1 & 0 \\ \frac{-1}{f_2} & 1 \end{bmatrix}\begin{bmatrix} 1 & x_2 \\ 0 & 1 \end{bmatrix}\begin{bmatrix} 1 & 0 \\ \frac{-1}{f_1} & 1 \end{bmatrix}\begin{bmatrix} 1 & x_1 \\ 0 & 1 \end{bmatrix}$$

$$i \cdot z_{o,Cavity} = \frac{i \cdot A \cdot Z_{o,Laser} + B}{i \cdot C \cdot Z_{o,Laser} + D} \Rightarrow \begin{Bmatrix} f_1 = 100 \\ f_2 = 200 \\ x_1 = 100 \\ x_2 = 300 \\ x_3 = 195.6 \end{Bmatrix}$$

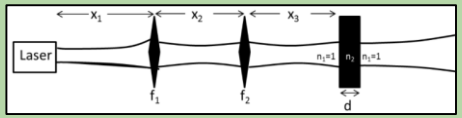

Fig. 12. A diagram showing the interaction of the beam with lenses and the first super mirror.

Fig. 12. The ray matrices [14] used to calculate [15] focal lengths and positions for our mode-matching lenses.

Acknowledgements:

This work was funded through NSF REU award #1852575, and the NASA South Dakota Space Grant Consortium. The authors would also like to thank John Dagit for his help configuring the laboratory and apparatus.

Citations:

[1]Hilke, H. J. (2010). Time projection chambers. *Reports on Progress in Physics,73*(11), 116201. doi:10.1088/0034-4885/73/11/116201
[2]Aprile, E., & Doke, T. (2010). Liquid xenon detectors for particle physics and astrophysics. *Reviews of Modern Physics,82*(3), 2053-2097. doi:10.1103/revmodphys.82.2053
[3] Mount, B. J., Hans, S., Rosero, R., Yeh, M., Chan, C., Gaitskel, R. J., ... Tvrznikova, L. (2017). LUX-ZEPLIN (LZ) Technical Design Report. Retrieved from: http: / hep.ucsb.edu/LZ/TDR/
[4] Berden, G., & Engeln, R. (Eds). (2009). *Cavity Ring-Down Spectroscopy: Techniques and Applications.* Chichester, West Sussex, UK: John Wiley & Sons Ltd.
[5] Busch, K., Busch, M. (Eds). (1999). *Cavity-Ringdown Spectroscopy: An Ultratrace-Absorption Measurement Technique.* Washington, DC: American Chemical Society
[6]Spence, T. G., Harb, C. C., Paldus, B. A., Zare, R. N., Willke, B., & Byer, R. L. (2000). A laser-locked cavity ring-down spectrometer employing an analog detection scheme. *Review of Scientific Instruments,71*(2), 347-353. doi:10.1063/1.1150206
[7]Berden, G., Peeters, R., & Meijer, G. (2000). Cavity ring-down spectroscopy: Experimental schemes and applications. *International Reviews in Physical Chemistry,19*(4), 565-607. doi:10.1080/01442350750040627
[8]O'Keefe, A., & Deacon, D. A. (1988). Cavity ring-down optical spectrometer for absorption measurements using pulsed laser sources. *Review of Scientific Instruments,59*(12), 2544-2551. doi:10.1063/1.1139895
[9] Crystal Technology, "Application note - Modulator model 3000 series," 1165AF-DIF0-4.0 datasheet, May 2010.
[10] Anderson, D. Z.; Frish, J. C.; Masser, C. S. Mirror reflectometer based on optical cavity decay time, *Appl. Opt.* 1984, **23**, 1238-1245.
[11]Khosrofian, J. M., & Garetz, B. A. (1983). Measurement of a Gaussian laser beam diameter through the direct inversion of knife-edge data. *Applied Optics,22*(21), 3406. doi:10.1364/ao.22.003406
[12]Araújo, M. A., Silva, R., Lima, E. D., Pereira, D. P., & Oliveira, P. C. (2009). Measurement of Gaussian laser beam radius using the knife-edge technique: Improvement on data analysis. Applied Optics, 48(2), 393. doi:10.1364/ao.48.000393
[13] Nachman, P., & Bernstein, A. (1996). Scanning spherical mirror Fabry-Perot interferometer: An upper division optics laboratory experiment. *American Journal of Physics*, 65 (3) 202-213. doi: 10.1119/1.18572
[14] Yariv, A. (1989). *Quantum electronics*. New York: J. Wiley.
[15] Siegman, A. E. (1986). *Lasers*. Mill Valley, CA: University Science Books.